

## Article

# Development and Application of Open Rotor Discrete Noise Prediction Program Using Time-Domain Methods

Hanyi Wang <sup>1,\*</sup>, Peng Shan <sup>1,\*</sup> and Yicheng Zhou <sup>2</sup><sup>1</sup> School of Energy and Power Engineering, Beihang University, Beijing 100191, China<sup>2</sup> Aero Engine Academy of China, Aero Engine Corporation of China, Beijing 101304, China; zhouyc@buaa.edu.cn

\* Correspondence: wanghanyi@buaa.edu.cn (H.W.); pshan@buaa.edu.cn (P.S.)

**Abstract:** The aerodynamic noise of an open rotor is one of the critical challenges that must be considered in its design and application. FODNOPP, a program specifically programmed to predict the aerodynamic discrete noise of single- and counter-rotating open rotors (such as propellers, propfans, and rotorcraft rotors) at subsonic, transonic, and supersonic helical blade tip speeds, has recently been developed by the first author. This program is composed of four prediction codes, namely code a1, code a2, code b, and code c, each based on Farassat-derived formulations Formu 1-RTE, Formu 1A, Formu 1-Sph, and Formu 3, providing time-domain solutions to the Ffowcs Williams–Hawkings equation. Four verification examples for both propeller low-speed flight noise and counter-rotating propfan take-off noise are presented, along with an application case for transonic helical tip speed counter-rotating propfan cruise noise. The results demonstrate the accuracy of FODNOPP in calculating the noise for these verification cases. And in the counter-rotating propfan cruise noise case, the maximum harmonic sound pressure level of the rear propfan is 5.5 dB higher than that of the front propfan. FODNOPP can be referred to as a comprehensive design tool, and it offers valuable guidance for engineering design focused on rotor-related noise reduction.

**Keywords:** discrete frequency noise; prediction program; time-domain method; counter-rotating propfans; retarded-time equation; transonic; acoustic planform; collapsing sphere; nonlinear harmonic method



**Citation:** Wang, H.; Shan, P.; Zhou, Y. Development and Application of Open Rotor Discrete Noise Prediction Program Using Time-Domain Methods. *Appl. Sci.* **2024**, *14*, 1138. <https://doi.org/10.3390/app14031138>

Academic Editors: Roberto Citarella, Luigi Federico and Venanzio Giannella

Received: 14 December 2023

Revised: 15 January 2024

Accepted: 17 January 2024

Published: 29 January 2024



**Copyright:** © 2024 by the authors. Licensee MDPI, Basel, Switzerland. This article is an open access article distributed under the terms and conditions of the Creative Commons Attribution (CC BY) license (<https://creativecommons.org/licenses/by/4.0/>).

## 1. Introduction

Aerodynamic noise, primarily discrete noise, associated with counter-rotating propfans, limits their application in civil aviation. Numerical prediction of this noise facilitates the development of noise reduction strategies during the early design phase of these propfans, thereby minimizing extensive noise testing later and reducing development costs. Moreover, aircraft equipped with counter-rotating propfan engines can comply with airworthiness certification noise standards and mitigate noise effects on aircrews, airport personnel, and surrounding communities. Thus, a method to predict the discrete noise of counter-rotating propfans under varying flight conditions, such as take-off, climb, and cruise, is urgently needed in China.

Aerodynamic discrete noise from open rotors can currently be computed using computer codes from abroad or commercial software. In 1992, NASA Langley Research Center (LaRC) developed the Advanced Subsonic and Supersonic Propeller Induced Noise prediction program (ASSPIN) [1,2], using Formu 1A [3] and Formu 3 [1], time-domain solutions of the Ffowcs Williams–Hawkings (FW–H) equation, as derived by Farassat. Previously, based on the two formulations along with Formu 1-RTE [4] and Formu 1-Sph [4], also from Farassat, LaRC had developed WOPWOP [3], as well as two modules of ANOPP [5], and DFP-ATP [6]. Formu 1-RTE and Formu 1A are optimally designed for predicting noise from open rotors at subsonic helical tip speeds, whereas Formu 1-Sph and Formu 3 are applicable for noise prediction across subsonic, transonic, and supersonic helical tip speeds. In 2003, the

German Aerospace Centre (DLR) developed APSIM [7], a program for subsonic open rotor aerodynamic noise prediction, based on the FW-H equation and the Kirchhoff formula, using an integral method and featuring a permeable surface function. For analyzing noise from open rotors with helical tip speeds near or beyond the speed of sound, numerical simulation software such as NUMECA FINE™/Acoustics 8.1 [8], the acoustic module of the software ANSYS Fluent 2021 R1 [9], and Actran 2020 [10] are applicable. However, these tools utilize a permeable surface integral method based on acoustic analogy, capturing noise from the turbulence within the permeable surface and near the rotor. Currently, no published literature about China's domestic program development for predicting the discrete noise of counter-rotating propfans, especially those with helical tip speeds across the speed of sound, is reported.

This study introduces FODNOPP, a self-developed program system for predicting the discrete noise of both single- and counter-rotating open rotors with subsonic/transonic/supersonic helical tip speeds. Its accuracy has been verified through four diverse case studies, along with a specific application for evaluating the cruise noise of the counter-rotating propfans with transonic helical tip speeds. FODNOPP is composed of four codes: code a1, code a2, code b, and code c, each successively utilizing formulations Formu 1-RTE, Formu 1A, Formu 1-Sph, and Formu 3, derived by Farassat. Both code a1 and code a2 employ two methodologies from the literature [5], one for calculating the retarded-time equation roots for subsonic acoustic source points on the blade surfaces of the single rotor and the other for transonic source points, which have been further improved in this study to better accommodate counter-rotating rotors. Observer points are synchronized with the airframe movement. The input data, namely the pressure distributions on the blade surfaces, are calculated using a formulation from [11] or calculated using the nonlinear harmonic (NLH) solver of the CFD software NUMECA FINE™/Turbo 14.2 [12]. FODNOPP calculates the discrete noise of open rotors by integrating across the solid wall surfaces of the blades, not considering the impact of the rotor flow field on noise propagation. Therefore, this approach might be less accurate for near-field noise predictions, or for noise from rotors with transonic helical tip speeds where turbulence effects may be notable. Nevertheless, FODNOPP is effective in directly evaluating open rotor noise and in conducting the geometry design of quieter rotors.

Utilizing four analytical formulations by Farassat, FODNOPP efficiently calculates the discrete frequency noise radiated by open rotors, ensuring high computational efficiency and broad selectivity. FODNOPP generates comprehensive data, including the acoustic pressure time histories and the spectra for thickness noise, load noise, and overall noise as a composite of the former two. The program also provides the A-weighted sound pressure level  $L_A$  in dBA, the effective perceived noise level  $EPNL$  in EPNdB, and other relevant acoustic engineering indices. When compared to the resource-intensive and time-consuming Computational AeroAcoustics (CAA) method, FODNOPP demonstrates certain advantages in computing the open-rotor noise. The four examples demonstrate that FODNOPP accurately computes the linear source discrete noise of diverse open rotors, including single propellers, propfans, counter-rotating propfans, rotorcraft rotors, and wind turbines, under a range of operating conditions.

## 2. Development of FODNOPP

The program name 'FODNOPP' (Fluid machinery department's Open rotor Discrete frequency NOise Prediction Program) is inspired by 'ANOPP' (NASA's Aircraft NOise Prediction Program), a program developed from the early 1970s to the mid 1980s [5]. In the two noise prediction codes utilizing Formu 1-RTE and Formu 1A, respectively, only the calculation of the acoustic pressure integral has partial differences, while the method for calculating the retarded time  $\tau$ , a crucial variable, is identical. Consequently, the corresponding codes are designated as FODNOPPa1 and FODNOPPa2, respectively. In contrast, in the other two codes employing Formu 1-Sph and Formu 3, respectively, their computations of the acoustic pressure integrals on the intersection curves between the blade surfaces and the collapsing sphere at a specified retarded time  $\tau \in [0, t]$  with the same method exhibit significant differences. Therefore, their respective codes are named FODNOPPb and FODNOPPc. Each of the four codes is capable of independently calculating noise from both single- and counter-rotating rotors.

To facilitate a comparative analysis and a cross-verification of the computation results for the same example obtained using distinct acoustic pressure formulations, this paper compares and categorizes the four time-domain formulations derived by Farassat. This study examines Brentner’s approach [3], which differentiates between far-field and near-field noise terms in Formu 1A, based on whether the denominators of the integrands include either the factor  $r$  or  $r^2$ . Specifically, in Formu 1A, the thickness and loading noise terms are bifurcated into far-field and near-field components, respectively. Similar to Formu 1A, this study applies Brentner’s method to divide Formu 1-RTE, Formu 1-Sph, and Formu 3 into the four distinct noise components and then contrasts the outcomes from the four formulations. The integral parts, along with the coefficients that consist exclusively of the variables  $\rho_0$  (denoting the density of the undisturbed medium) and  $c_0$  (denoting the speed of sound), are extracted and catalogued for the four noise components, as detailed in Table 1. Notably, the thickness noise terms in Formu 1-RTE and Formu 1-Sph consist solely of the far-field component and no near-field counterpart. The comparison of the coefficients of each noise component of Formu 1-RTE and Formu 1-Sph, as presented in part c of Table 1, indicates that, for each component, the product of Formu 1-Sph’s integral part and  $c_0$  should be equal to the integral part of its corresponding component in Formu 1-RTE.

**Table 1.** Integral parts and coefficients of noise component terms of Formu 1-RTE [4], Formu 1A [3], Formu 1-Sph [4], and Formu 3 [1]: (a) Integral parts of thickness noise term; (b) Integral parts of loading noise term; (c) Coefficients of both noise terms.

| (a)         |  |  |                                |                            |
|-------------|--|--|--------------------------------|----------------------------|
| Formulation | Far-Field Thickness  | Near-Field Thickness   |                                |                            |
| Formu 1-RTE | $\int_{f=0} \left[ \frac{v_n}{r(1-M_r)} \right]_{ret} dS$ (Differentiation required)   | \  |                                |                            |
| Formu 1A    | $\int_{f=0} \left[ \frac{v_n}{r(1-M_r)^2} + \frac{v_n M_i \hat{r}_i}{r(1-M_r)^3} \right]_{ret} dS$   | $\int_{f=0} \left[ \frac{v_n(M_r - M^2)}{r^2(1-M_r)^3} \right]_{ret} dS$                             |                                |                            |
| Formu 1-Sph | $\int_{f,g=0} \frac{v_n}{r \sin \theta} d\Gamma d\tau$ (Differentiation required)  | \  |                                |                            |
| Formu 3     | $\int_{f,g=0} \int_{k>0} \frac{1}{r} \cdot \frac{M_n^2 Q_E + Q_E' + Q_E''}{\sin \theta} d\Gamma d\tau$<br>$- \int_{f,g,k=0} \frac{1}{r} \cdot \frac{M_n^2 Q_E + M_n M_{av}}{ \cos \varphi } d\tau$                                   | $\int_{f,g=0} \int_{k>0} \frac{1}{r^2} \cdot \frac{M_n^2 Q_N'}{\sin \theta} d\Gamma d\tau$           |                                |                            |
| (b)         |  |  |                                |                            |
| Formulation | Far-Field Loading  | Near-Field Loading   |                                |                            |
| Formu 1-RTE | $\int_{f=0} \left[ \frac{l_r}{r(1-M_r)} \right]_{ret} dS$ (Differentiation required)   | $\int_{f=0} \left[ \frac{l_r}{r^2(1-M_r)} \right]_{ret} dS$  |                                |                            |
| Formu 1A    | $\int_{f=0} \left[ \frac{l_i \hat{r}_i}{r(1-M_r)^2} + \frac{l_r M_i \hat{r}_i}{r(1-M_r)^3} \right]_{ret} dS$   | $\int_{f=0} \left[ \frac{-l_i M_i}{r^2(1-M_r)^2} + \frac{l_r(1-M^2)}{r^2(1-M_r)^3} \right]_{ret} dS$ |                                |                            |
| Formu 1-Sph | $\int_{f,g=0} \frac{l_r}{r \sin \theta} d\Gamma d\tau$ (Differentiation required)  | $\int_{f,g=0} \frac{l_r}{r^2 \sin \theta} d\Gamma d\tau$   |                                |                            |
| Formu 3     | $\int_{f,g=0} \int_{k>0} \frac{1}{r} \cdot \frac{p Q_E + \frac{\lambda}{c_0} \dot{p}_B - b \frac{\partial p_B}{\partial c_n}}{\sin \theta} d\Gamma d\tau$<br>$- \int_{f,g,k=0} \frac{1}{r} \cdot \frac{p Q_E}{ \cos \varphi } d\tau$ | $\int_{f,g=0} \int_{k>0} \frac{1}{r^2} \cdot \frac{p Q_N'}{\sin \theta} d\Gamma d\tau$               |                                |                            |
| (c)         |  |  |                                |                            |
| Formulation | Far-Field Thickness  | Near-Field Thickness   | Far-Field Loading              | Near-Field Loading         |
| Formu 1-RTE | $\frac{\rho_0}{4\pi}$  | \  | $\frac{1}{4\pi c_0}$           | $\frac{1}{4\pi}$           |
| Formu 1A    | $\frac{\rho_0}{4\pi}$  | $\frac{\rho_0 c_0}{4\pi}$  | $\frac{1}{4\pi c_0}$           | $\frac{1}{4\pi}$           |
| Formu 1-Sph | $\frac{\rho_0}{4\pi} \cdot c_0$  | \  | $\frac{1}{4\pi c_0} \cdot c_0$ | $\frac{1}{4\pi} \cdot c_0$ |
| Formu 3     | $\frac{\rho_0 c_0^3}{4\pi}$  | $\frac{\rho_0 c_0^3}{4\pi}$  | $\frac{c_0}{4\pi}$             | $\frac{c_0}{4\pi}$         |

### 3. Verification of Accuracy of FODNOPP

To evaluate the accuracy of FODNOPP, namely code a1, code a2, code b, and code c, this study conducts calculations with two examples to predict noise from the flight propeller PROP [11], and another two examples to predict noise from the counter-rotating propfan model CRPFt, with a diameter  $D = 0.622$  m, operating at the take-off conditions of an altitude  $H = 300$  m and a flight Mach number  $M = 0.24$ .

#### 3.1. Rotor Geometry Model and Observer Point Coordinates

Figure 1 depicts the propeller PROP [11] and the counter-rotating propfan models CRPFt and CRPFc [13] along with the pressure distributions on their blade surfaces. Among them, only PROP and CRPFt are utilized in the code verifications. In 2016, based on the compressible lifting surface theory, Zhou [13] developed an inverse design problem approach and achieved the design of CRPFc at a cruise point with an altitude  $H = 11$  km and a flight Mach number  $M = 0.8$ . Now, this paper meticulously recalibrates the orientations of the front and rear propfans of CRPFc by resetting the pitch angles of two airfoil sections, at a relative radius of  $r/R = 0.75$ , to  $37.9^\circ$  for the front propfan blades and to  $37.4^\circ$  for the rear propfan blades, respectively. Via this calibration, CRPFt is derived, specifically for the noise prediction under the take-off conditions at an altitude  $H = 300$  m and a flight Mach number  $M = 0.24$ . The two pitch angles chosen correspond to those employed in the wind tunnel experiments by Sullivan [14], in which the counter-rotating propfan model F7A7 at an incoming Mach number  $M = 0.24$  is tested. The pressure distributions on the blade surfaces of PROP are directly derived from the specific load distribution equation presented in [11]. In contrast, for CRPFt and CRPFc, the time-dependent pressure distributions on the surfaces of each blade are reconstructed from the approximate unsteady solutions of the flow fields simulated by the NLH solver. The blades of the front propfan have one distinct time sequence, while the blades of the rear propfan have another distinct time sequence. We take the time interval between the maximum moment and the minimum moment in the discrete-time sequence to be equal to the change cycle of the pressure of the blade surface. This pressure reconstruction process enables capturing the pressure distributions at each moment within these respective time sequences for each propfan. The pressure distributions on the blades of CRPFt and CRPFc, at  $t = 0$  s, are shown in Figure 1b,c, in which the plain blades are the reference blades F1t, R1t, F1c, and R1c. (F, R, B, 1, t, and c denote, respectively, the blade of front propfan of either CRPFt or CRPFc, blade of rear propfan of either CRPFt or CRPFc, blade of PROP, first blade, take-off conditions, and cruise conditions).

In the flow field simulations, the coordinate system of the model may differ from that used in the acoustic calculations. In the software NUMECA FINE™/Turbo 14.2, the incoming flow is oriented along the  $+z$  axis, so the flight direction of the rotor is along the  $-z$  axis, as illustrated in Figure 1b,c. In the orthogonal coordinate systems  $Oxyz$ , shown in Figure 1a–c, the geometric centers of PROP, the front propfan of CRPFt, and the front propfan of CRPFc are all situated at their respective origin  $O$ , and their rotor discs lie within their respective  $Oxy$  plane. Additionally, the pitch change axes of the reference blades B1 of PROP, F1t of CRPFt, and F1c of CRPFc coincide with their respective  $+y$  axis, while the pitch change axes of the reference blades R1t of CRPFt and R1c of CRPFc are parallel to their respective  $+y$  axis. In the noise calculation using FODNOPP, the flight direction of the rotor is set along the  $+z$  axis, and, at time  $t = 0$  s, the pitch change axes of the reference blades B1, F1t, and F1c coincide with their respective  $+y$  axis. The parameters for the noise calculations, including the flight speeds, rotational speeds, and noise observer coordinates for PROP, CRPFt, and CRPFc, are detailed in Table 2. The observer coordinates, set at  $O(0, 7.28 \text{ m}, 0)$ , align with those employed in [11], ensuring consistency in the comparative analysis.

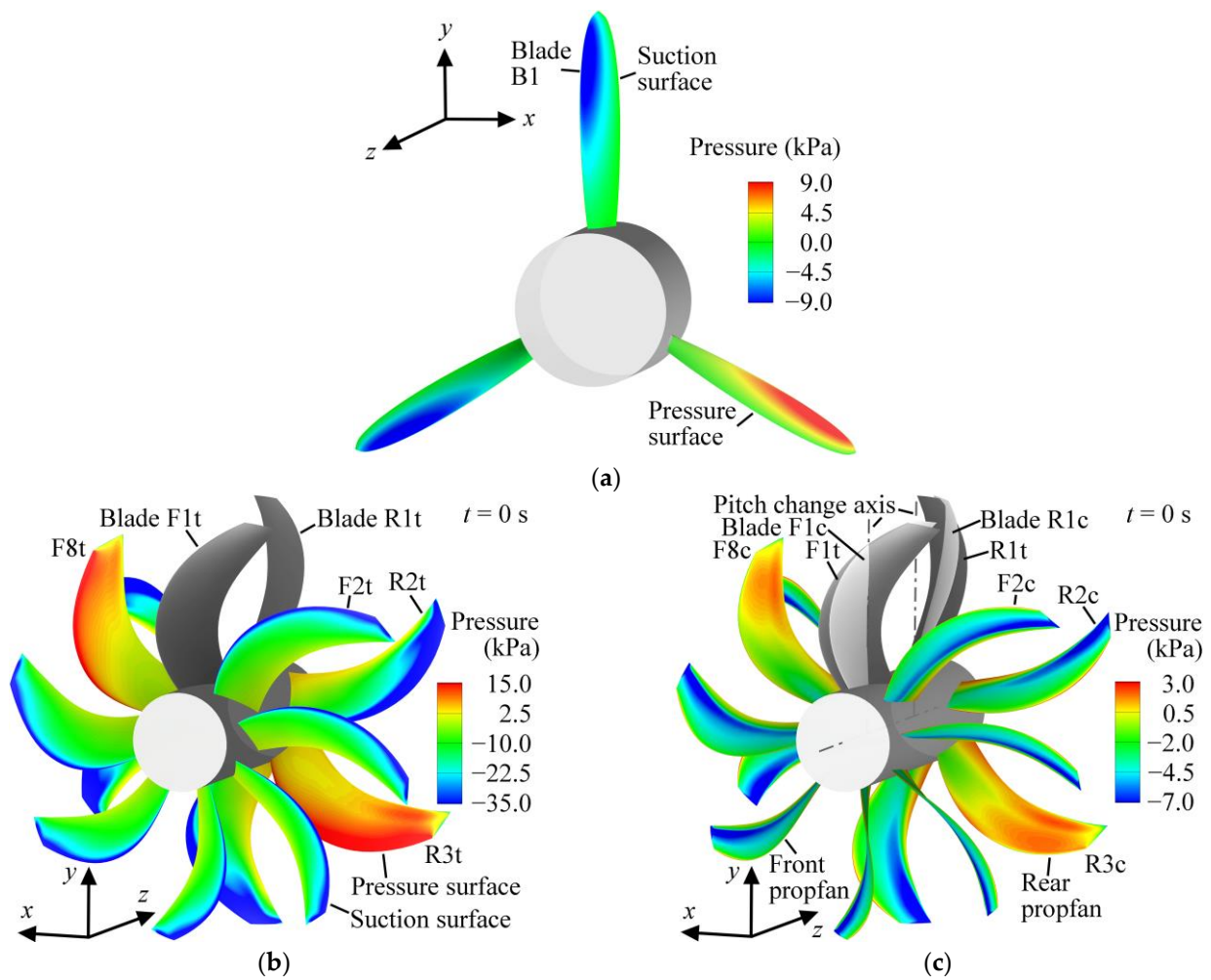


**Figure 1.** Geometry and pressure distributions on blade surfaces of: (a) Propeller PROP [11]; (b) Counter-rotating propfans CRPFt; (c) Counter-rotating propfans CRPFc [13].

**Table 2.** Key flight, geometry, and motion parameters, and noise observer coordinates for open rotors PROP, CRPFt, and CRPFc.

| Parameter   | Propeller (PROP)  | Counter-Rotating Propfans at Take-Off (CRPFt) |              | Counter-Rotating Propfans at Cruising (CRPFc) |              |
|---|-------------------|---|--------------|---|--------------|
|   |                   | Front Propfan                                 | Rear Propfan | Front Propfan                                 | Rear Propfan |
| Flight altitude $H$ (m)   | 0                 | 300   |              | 11,000  |              |
| Flight Mach number $M$  | 0.12              | 0.24  |              | 0.8   |              |
| Flight speed $v_x, v_y, v_z$ (m/s)  | 0, 0, +40.14      | 0, 0, +81.39                                  |              | 0, 0, +236.1                                  |              |
| Speed of sound $c_0$ (m/s)  | 345               | 339.141                                       |              | 295.107                                       |              |
| Number of blades $N_b$  | 3                 | 8   | 6            | 8   | 6            |
| Blade tip diameter $D = 2R$ (m)   | 2.6               | 0.622   | 0.622        | 0.622   | 0.622        |
| Hub radius $r_h$ (m)  | 0.358             | 0.072   | 0.072        | 0.072   | 0.072        |
| Pitch angle, $\varphi_{0.75}$ ( $^\circ$ ), of airfoil section at relative radius of $\bar{r} = r/R = 0.75$ | 9.3               | 37.9  | 37.4         | 58.3  | 55.3         |
| Revolution $n$ (r/min)  | +2145             | +9814.37                                      | −9814.37     | +7246.4                                       | −7246.4      |
| Helical-tip Mach number $M_{Hel}$   | 0.854             | 0.97  | 0.97         | 1.13  | 1.13         |
| Observer coordinates $O(x, y, z)$ (m)   | $O_1(0, 7.28, 0)$ | $O_1(0, 0.4665, 0), O_2(0, 7.28, 0)$          |              | $O_1(0, 7.28, 0)$                             |              |

### 3.2. Example Verifications for Program Accuracy

#### 3.2.1. Subsonic Single Propeller, Using Code a2

To validate code a2, the prediction example of the forward flight propeller noise provided by Farassat and Brown [11] is selected, in which the experimental and theoretical results for overall noise, encompassing acoustic pressure time histories and spectra, are presented. Separately, Woan and Gregorek [15] presented theoretical results, including the acoustic pressure time histories and spectra, for the overall noise as well as for its thickness and loading noise components. In this paper, the acoustic pressure time history and spectrum of the overall noise at the observer point  $O_1$  (0, 7.28 m, 0) are calculated using code a2. These results are then benchmarked against the experimental data sourced from Farassat and Brown, as well as the theoretical results provided by Farassat and Brown and those by Woan and Gregorek, as depicted in Figure 2. Additionally, the thickness and loading noise results using code a2 are contrasted with those by Woan and Gregorek in Figure 3. Both Figures 2 and 3 demonstrate that the results of code a2 align well with the experimental data in [11] and the theoretical results in [11,15]. This substantiates the efficacy of code a2 in accurately predicting the overall noise for the propeller with a subsonic helical tip speed and also in determining its thickness and loading noise components.

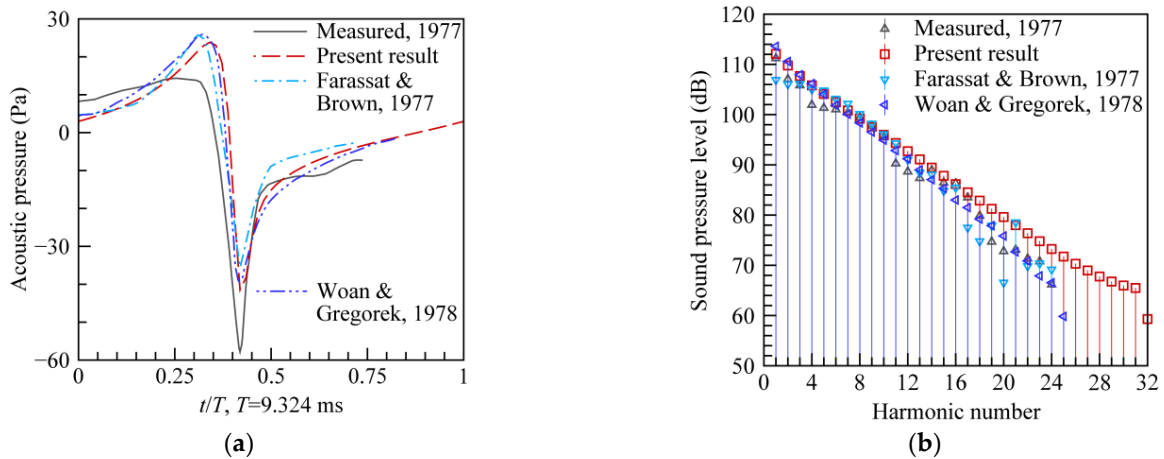


**Figure 2.** Overall noise of propeller PROP at sea level  $H = 0$  m, flight Mach number  $M = 0.12$ , at observer point  $O_1$  (0, 7.28 m, 0) using code a2, compared with that tested in [11] and calculated in [11,15]: (a) Acoustic pressure time histories; (b) Spectra (blade passing frequency BPF = 107.25 Hz).

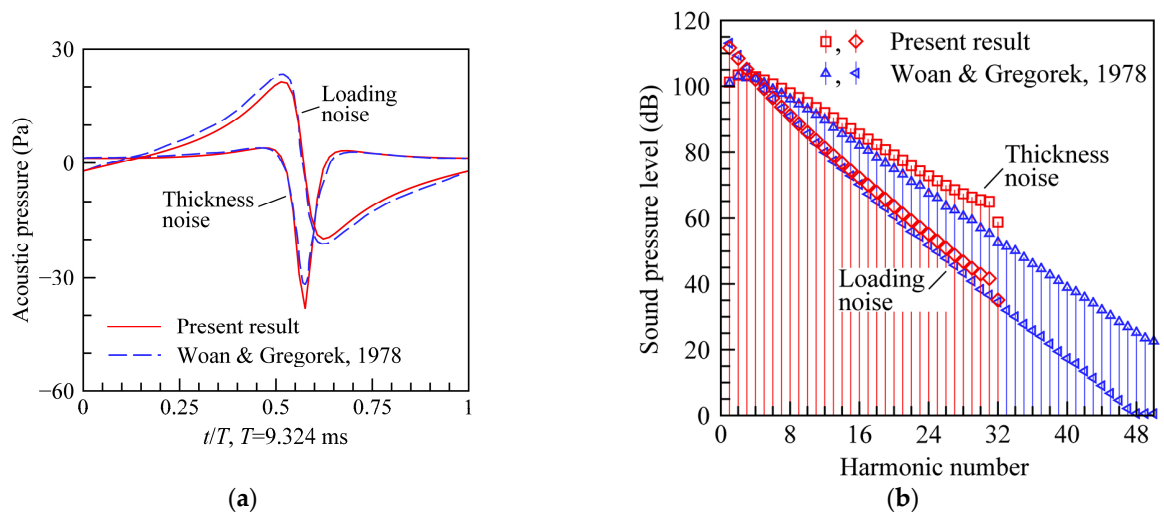


**Figure 3.** Thickness noise and loading noise of propeller PROP at sea level  $H = 0$  m, flight Mach number  $M = 0.12$ , at observer point  $O_1$  (0, 7.28 m, 0) using code a2, compared with those calculated in [15]: (a) Acoustic pressure time histories; (b) Spectra (BPF = 107.25 Hz).

### 3.2.2. Subsonic Single Propeller, Using Code a1, Code b, and Code c

To verify the accuracy of the three codes a1, b, and c in calculating the noise of a single propeller, the same propeller noise prediction case as in Section 3.2.1 is independently recalculated using code a1 (Formu 1-RTE), code b (Formu 1-Sph), and code c (Formu 3). The acoustic pressure time histories and spectra of the overall noise at the observer point  $O_1$  (0, 7.28 m, 0), obtained via code a1, code b, and code c, are compared with those obtained via code a2, as depicted in Figure 4. This figure indicates that the results from code a1, code a2, and code b overall demonstrate a high level of consistency, with the results between code a1 and code b showing an even higher degree of agreement, particularly in terms of the acoustic pressure time histories. The acoustic pressure time history of the overall noise, as obtained by using code c, follows the same trend as that by using code a2. However, the accuracy of the results from code c requires improvement. The reliability of code a1, code b, and code c in predicting the discrete frequency noise of a propeller with a subsonic helical tip speed has been verified to a certain extent.

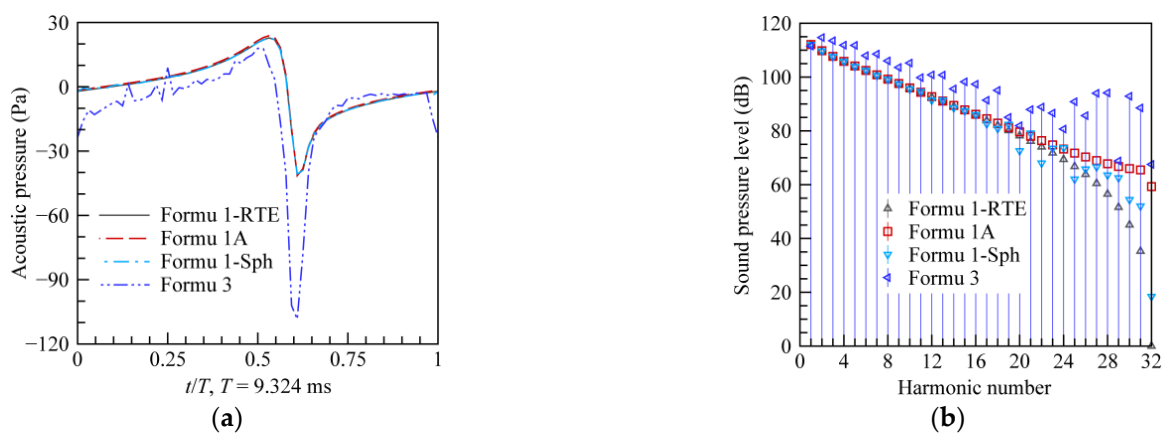


**Figure 4.** Overall noise of propeller PROP at sea level  $H = 0$  m, flight Mach number  $M = 0.12$ , at observer point  $O_1$  (0, 7.28 m, 0) separately by using Formu 1-RTE, Formu 1-Sph, and Formu 3, compared with that by using Formu 1A: (a) Acoustic pressure time histories; (b) Spectra (BPF = 107.25 Hz).

### 3.2.3. Subsonic Counter-Rotating Propfans, Using Code a2

The three-dimensional unsteady flow field of the counter-rotating propfan model CRPFt, under take-off conditions at an altitude  $H = 300$  m and a flight Mach number  $M = 0.24$ , is accurately simulated using the NLH solver of NUMECA FINE™/Turbo. Utilizing Aeroacoustics [16], an optional module also based on Formu 1A, integrated within the solver for the discrete frequency noise calculation, the noises at the observer point  $O_1$  (0, 0.4665 m, 0), positioned directly above the front propfan with a distance  $1.5R$  from the rotor axis, including the overall noise and its thickness and loading noise components, all generated by the front, the rear, and both propfans of CRPFt, respectively, are calculated accurately. Through the above two processes, the acoustic pressure time history and spectrum of the overall noise generated collectively by the front and rear propfans of CRPFt are obtained. The results are then compared with those obtained using code a2, as depicted in Figure 5. This figure, along with its detailed description [17], indicates a high degree of congruence of the acoustic pressure time histories. Since the negative sound pressure levels are not practically meaningful, the sound pressure levels of the tones, particularly for the frequencies up to 32 times the rotor shaft frequency, show a considerable degree of similarity across both methods. Thereby, the accuracy of code a2, in predicting the noise of counter-rotating propfans with subsonic helical tip speeds, is effectively demonstrated.

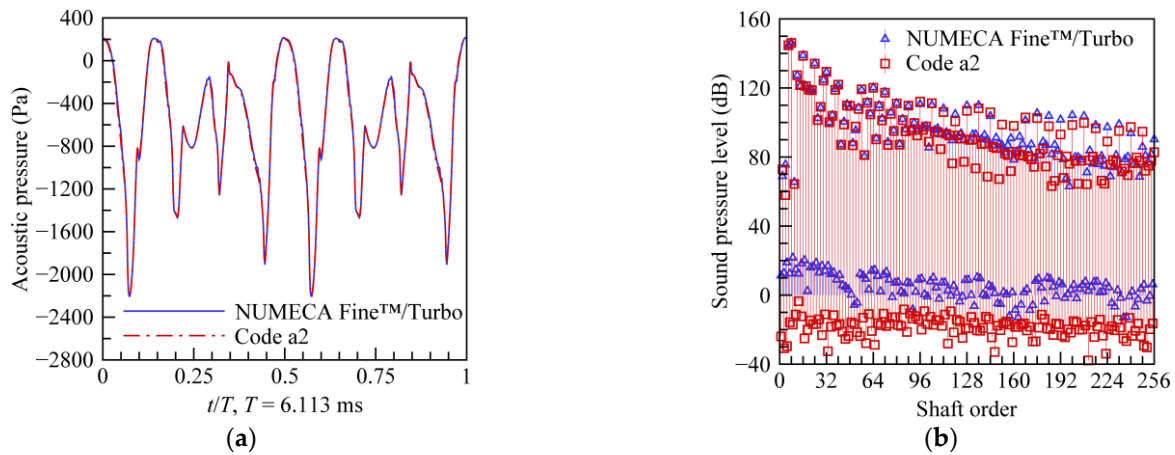


**Figure 5.** Overall noise of counter-rotating propfans CRPFt at take-off altitude  $H = 300$  m, flight Mach number  $M = 0.24$ , at observer point  $O_1 (0, 0.4665 \text{ m}, 0)$  using code a2, compared with that using NUMECA Fine™/Turbo: (a) Acoustic pressure time histories; (b) Spectra (rotor passing frequency RPF = 163.57 Hz).

### 3.2.4. Subsonic Counter-Rotating Propfans, Using Code a1 and Code b

The overall noise generated collectively by both propfans of CRPFt at the observer point  $O_2 (0, 7.28 \text{ m}, 0)$ , under the take-off conditions at an altitude  $H = 300$  m and a flight Mach number  $M = 0.24$ , is separately calculated using code a1 and code b. The results of each are depicted in Figure 6. The comparative analysis indicates that the acoustic pressure time histories from the two codes show a similar trend. Moreover, the sound pressure levels of the dominant tones, with the frequencies up to 32 times the rotor shaft frequency, are nearly equal. In this case, while code a1 provides a more accurate and smoother acoustic pressure time history compared to code b, the method of code b involves the intricate  $\Gamma$ -curves at a specified retarded time  $\tau$  within the interval  $[0, t]$ , with the possibility of presence or absence. These  $\Gamma$ -curves result from the varied intersection forms between the blade surfaces and the collapsing sphere. At a specified time  $\tau$  within  $[0, t]$ , the complexity of the intersection form may necessitate further improvement in the accuracy of the  $\Gamma$ -curves, if  $\Gamma$ -curves are present. Therefore, it can be concluded that the results from code a1 and code b, in calculating the discrete frequency noise of counter-rotating propfans with subsonic helical tip speeds, are in agreement.

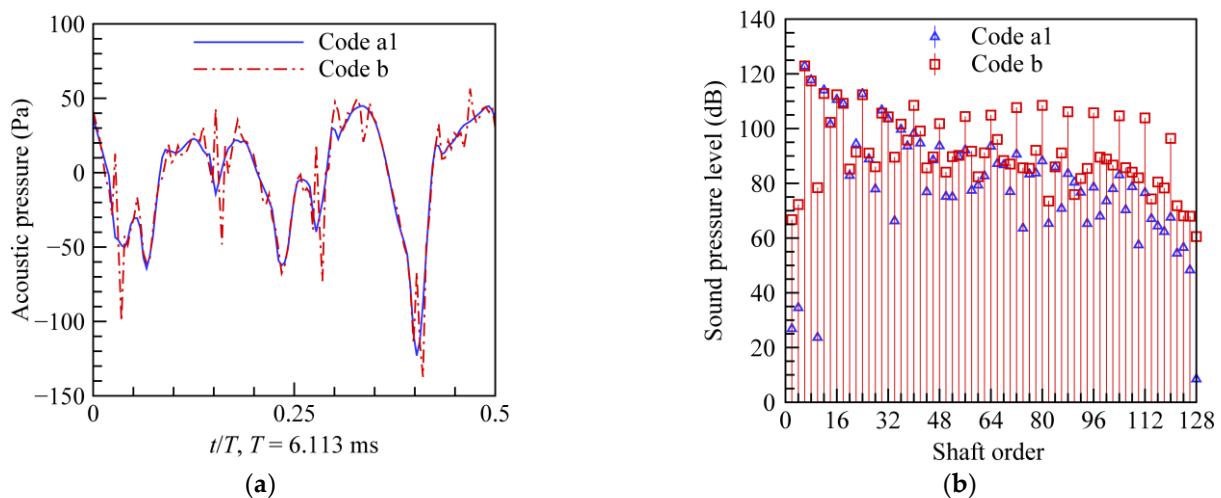


**Figure 6.** Overall noise of counter-rotating propfans CRPFt at take-off altitude  $H = 300$  m, flight Mach number  $M = 0.24$ , at observer point  $O_2 (0, 7.28 \text{ m}, 0)$  using code b, compared with that using code a1: (a) Acoustic pressure time histories; (b) Spectra (RPF = 163.57 Hz).

The results from the four aforementioned noise examples, including two subsonic single-rotating cases and two subsonic counter-rotating cases, are subjected to a further analysis. Code a1 and code a2, based on Formu 1-RTE and Formu 1A, respectively, differ mainly in several variables within the integrands of the acoustic pressure integrals, the coefficients of these integrals, and whether or not the first-order partial differentiation with respect to the observer time  $t$  is performed. Other than these differences, the two codes employ the same methods and the same algorithms in calculating the retarded times  $\tau$  and in integrating the control variables for the acoustic pressure calculation of the rear propfan. Therefore, it is presumed that code a1 is also capable of accurately calculating the noise of counter-rotating open rotors at subsonic helical tip speeds. Due to the results calculated using code a1 and code b showing a degree of agreement regarding the noise of CRPFt under take-off conditions, code b is somewhat accurate in computing the noise of counter-rotating open rotors at subsonic helical tip speeds. Code b and code c, based on Formu 1-Sph and Formu 3, respectively, differ mainly regarding several variables within the integrands of the acoustic pressure integrals, the coefficients of these integrals, and whether or not the first-order partial differentiation with respect to the observer time  $t$  is performed. Other than these differences, the two codes employ the same methods and the same algorithms in calculating the intersection  $\Gamma$ -curves between the blade surfaces and the collapsing sphere and in integrating the control variables for the acoustic pressure calculation of the rear propfan. Therefore, it is presumed that code c is also capable of accurately calculating the noise of counter-rotating open rotors at subsonic helical tip speeds. Due to code a1 and code a2 effectively solving the retarded-time equations for acoustic source points at transonic helical speeds, they can calculate the noise of rotors at transonic and supersonic helical tip speeds. The above verifications have shown that code a1, code a2, code b, and code c can provide accurate noise assessments for rotors at subsonic helical tip speeds, so it is derived that these codes are also capable of calculating noise of rotors at transonic and supersonic helical tip speeds. However, from experience, the noise data of rotors at transonic helical tip speeds computed using code a2 indicate a significant lack of accuracy; therefore, the application of code a2 for the rotors at transonic or supersonic helical tip speeds is discouraged. The comprehensive analyses presented here conclusively establish that the suite of the four FODNOPP codes can accurately compute the discrete frequency noise associated with single- and counter-rotating open rotors at subsonic/transonic/supersonic helical tip speeds.

#### **4. Application of FODNOPP for Transonic Counter-Rotating Propfans at Cruising**

##### **4.1. Aerodynamic Discrete Noise of Counter-Rotating Propfans CRPFc with Transonic Helical Tip Speed**

The overall noise generated by the front, the rear, and both propfans of the counter-rotating propfan model CRPFc featuring a transonic helical tip speed is separately calculated at cruise altitude  $H = 11$  km and flight Mach number  $M = 0.8$ , as shown in Figure 7. These calculations are conducted independently using code a1 and code b at the observer point  $O_1 (0, 7.28 \text{ m}, 0)$ , which moves in synchronization with the fuselage and is situated in the plane of the front propfan disc, maintaining a minimum distance of 11.2 times the rotor diameter from the blade tip. Figure 7 shows that the acoustic pressure time histories from both codes exhibit similar trends, and the sound pressure levels of the low-order harmonics, with the frequencies not exceeding 16 times the rotor shaft frequency, are also comparable. According to the results from code b, the maximum harmonic sound pressure level of the overall noise of both propfans of CRPFc is 112.5 dB. Furthermore, the maximum harmonic sound pressure level of the overall noise of the front propfan is 5.5 dB lower than that of the rear propfan. Code a1 employs the method of solving the multiple roots of the retarded-time equations of the acoustic source points at transonic helical speeds, thereby achieving a computational efficiency that is markedly superior to that of code b. However, this approach leads to more fluctuating acoustic pressure time histories and reduces the accuracy of the results. Consequently, when seeking greater accuracy of the

discrete noise of the counter-rotating propfans with transonic helical tip speeds, code b is the preferred option.

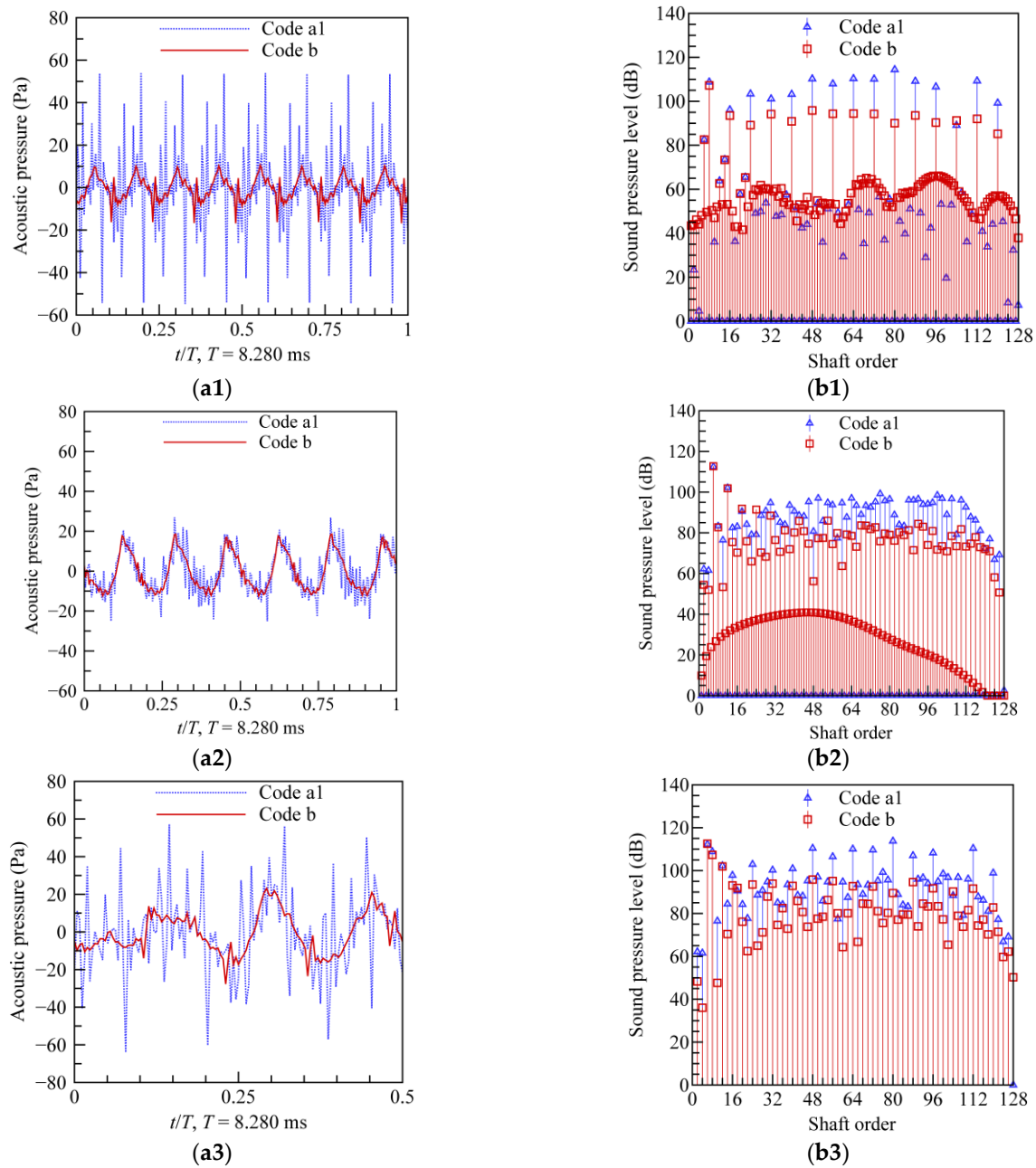


**Figure 7.** Overall noise of counter-rotating propfans CRPFc at cruise altitude  $H = 11$  km, flight Mach number  $M = 0.8$ , at observer point  $O_1 (0, 7.28 \text{ m}, 0)$  separately using code a1 and code b for front (a1,b1), rear (a2,b2), and both propfans (a3,b3) of CRPFc: (a1–a3) Acoustic pressure time histories; (b1–b3) Spectra (RPF = 120.77 Hz).

#### 4.2. Three Critical Variables in Noise Calculation for Propfans with Transonic Helical Tip Speed

FODNOPP effectively computes the three essential variables: (1) the roots  $\tau$  of the retarded-time equations of acoustic source points, each at a helical speed that is either subsonic or transonic; (2) the intersection curves  $\Gamma$  of the blade surfaces with the collapsing sphere at a specified  $\tau$ , within the range  $[0, t]$ ; and (3) the algebraic term  $\partial p_B / \partial \sigma_b$  in Formu 3. Figure 8 illustrates the solution schematics of the three variables, corresponding to the noise calculation at  $t = 5.75T$ , where  $T = 8.280$  ms, as calculated in Section 4.1. As inferred from the periodic nature of the acoustic pressure time histories, the acoustic pressures at

$t = 5.75T$  are equivalent to those at the moments  $t/T = 0.75$  in Figure 7(a1,a2) and  $t/T = 0.25$  in Figure 7(a3).

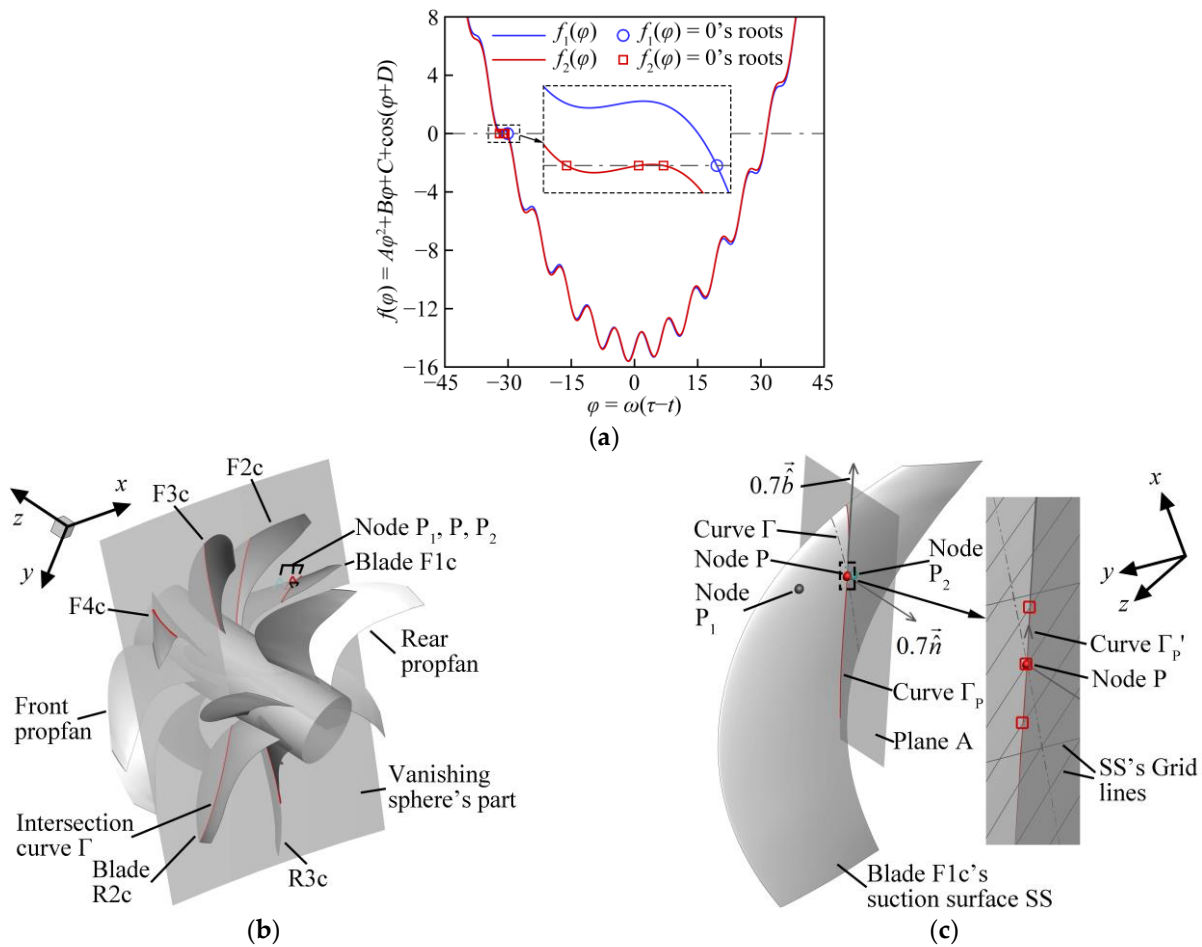


**Figure 8.** Schematic representations of three key variables solved using FODNOPP: (a) Roots of transonic retarded-time equations; (b) Intersection curves of counter-rotating propfans with collapsing sphere; (c) Algebraic term  $\partial p_B / \partial \sigma_b$  in Formu 3.

The source nodes,  $P_1$  and  $P_2$ , located on the suction surface of blade F1c, are identified with coordinates  $(0.24, 0.8)$  and  $(0.62, 0.8)$ , respectively, in terms of  $(x/c, r/R)$ . The retarded-time equations of nodes  $P_1$  and  $P_2$  are determined as  $f_1(\varphi) = 0$  and  $f_2(\varphi) = 0$ , respectively. Results reveal that the two equations have one and three real roots, respectively, as illustrated in Figure 8a. The helical Mach numbers, denoted as  $M_{Hel}$ , for  $P_1$  and  $P_2$  are 1.02. Here, for the airfoil section at a relative radius  $r/R$ , the  $x$  denotes the chordwise distance from a node to the leading edge, and  $c$  denotes the chord length. At the retarded time  $\tau = 0.7T$  for  $t = 5.75T$ , in CRPFc, only the blades F1c, F2c, F3c, and F4c of the front propfan, along with the blades R2c and R3c of the rear propfan, intersect with the collapsing sphere surface, as illustrated in Figure 8b. The sphere is centered at  $O_{1v} (0, 7.28 \text{ m}, 0 + v_z t \text{ m}) = O_{1v} (0, 7.28 \text{ m}, 11.23 \text{ m}) = O_{1v} (0, 11.70D, 18.05D)$  and has a radius  $r_s = c_0(t - \tau) = 12.33 \text{ m} = 19.82D$ .

In Figure 8b, on the intersection curve  $\Gamma$  of the suction surface of blade F1c with the sphere surface, the node  $P$  is selected as the node most adjacent to the airfoil section at  $r/R = 0.8$ . Here, ‘node’ denotes the point where one grid line of the blade surface intersects with the sphere surface or its normal plane. To compute  $\partial p_B / \partial \sigma_b$  at  $P$ , it is essential to first determine the intersection curve  $\Gamma_P$ , as shown in Figure 8c, on which  $p_B$  and  $\sigma_b$  are the variables at each node. Here,  $\Gamma_P$  is the intersection curve of plane A with F1c’s suction surface. Plane A is a normal plane of F1c’s suction surface at  $P$ , defined by the tangent

vector  $\vec{b}$  and the normal vector  $\vec{n}$  of F1c's suction surface at P.  $p_B$  denotes the pressure at each node of the curve  $\Gamma_P$  in the blade-fixed coordinate system, while  $\sigma_b$  denotes the length of the curve on  $\Gamma_P$ , extending from the starting node to each node on  $\Gamma_P$ . Tangent vector  $\vec{b}$  is equal to  $\lambda \vec{M}_i$  plus  $\lambda_1 \vec{t}_1$ .  $\vec{b}$  and  $\vec{n}$  are, respectively, the unit vectors of  $\vec{b}$  and  $\vec{n}$ . The meanings of  $\lambda$ ,  $\lambda_1$ ,  $\vec{M}_i$ , and  $\vec{t}_1$  are provided in [1]. To optimize computational efficiency,  $\partial p_B / \partial \sigma_b$  is calculated using the pressure and coordinates of node P, as well as those of the two nodes adjacent to P on curve  $\Gamma_P$ . The curve  $\Gamma_{P'}$ , a segment of curve  $\Gamma_P$ , which includes these three nodes, is depicted in Figure 8c.

The above results indicate that for a transonic source, the retarded times  $\tau$  have only 0, 1, or 3 solutions of distinct values. Considering the complexity of the curved blade surfaces, the accuracies of the intersection curve  $\Gamma$  and the tangent vector  $\vec{b}$ , calculated numerically, are vital for the accuracy of the acoustic pressure. Consequently, a continuous optimization of code b and code c is needed to improve the accuracies of  $\Gamma$  and  $\vec{b}$ .

## 5. Conclusions

Based on the four time-domain solution formulations derived by Farassat, the recently developed FODNOPP, with four corresponding codes, can accurately calculate aerodynamic discrete noise for single- and counter-rotating open rotors with subsonic/transonic/supersonic helical tip speeds.

The maximum harmonic sound pressure level of the overall noise generated by both propfans of the counter-rotating propfan model CRPFc, with a transonic helical tip Mach number 1.13, is 112.5 dB. Furthermore, the maximum harmonic sound pressure level of the overall noise of the front propfan of CRPFc is 5.5 dB lower than that of the rear propfan.

FODNOPP is crucial for exploring the aerodynamic acoustic characteristics of single- and counter-rotating propellers, propfans, and rotorcraft rotors. It is vital for the low-noise design of open rotors in the aerodynamic inverse design problem phase.

The calculation accuracy of the intersection curves between the blade surfaces and the collapsing sphere in code b and code c requires further enhancement. Additionally, integrating a module of the permeable surface method for computing open-rotor aerodynamic noise into FODNOPP is a potential advancement.

**Author Contributions:** Methodology, H.W. and P.S.; program, H.W.; CRPFc geometry, Y.Z.; validation, H.W.; writing—original draft preparation, H.W.; writing—review and editing, P.S. All authors have read and agreed to the published version of the manuscript.

**Funding:** This research received no external funding.

**Institutional Review Board Statement:** Not applicable.

**Informed Consent Statement:** Not applicable.

**Data Availability Statement:** The data presented in this study are available upon request from the corresponding author. The data are not publicly available due to privacy.

**Conflicts of Interest:** Author Yicheng Zhou was employed by the company Aero Engine Corporation of China. The remaining authors declare that the research was conducted in the absence of any commercial or financial relationships that could be construed as a potential conflict of interest.

## References

1. Dunn, M.H.; Tarkenton, G.M. *Computational Methods in the Prediction of Advanced Subsonic and Supersonic Propeller Induced Noise—ASSPIN Users' Manual*; NASA CR-4434; NASA LaRC: Hampton, VA, USA, 1992.
2. Farassat, F.; Dunn, M.H.; Spence, P.L. Advanced propeller noise prediction in the time domain. *AIAA J.* **1992**, *30*, 2337–2340. [[CrossRef](#)]
3. Brentner, K.S. *Prediction of Helicopter Rotor Discrete Frequency Noise—A Computer Program Incorporating Realistic Blade Motions and Advanced Acoustic Formulation*; NASA TM-87721; NASA LaRC: Hampton, VA, USA, 1986.
4. Nystrom, P.A.; Farassat, F. *A Numerical Technique for Calculation of the Noise of High-Speed Propellers with Advanced Blade Geometry*; NASA TP-1662; NASA LaRC: Hampton, VA, USA, 1980.

5. Zorumski, W.E.; Weir, D.S. *Aircraft Noise Prediction Program Theoretical Manual: Part 3—Propeller Aerodynamics and Noise*; NASA TM-83199; NASA LaRC: Hampton, VA, USA, 1986.
6. Dunn, M.H.; Tarkenton, G.M. *Users' Manual for the Langley High Speed Propeller Noise Prediction Program (DFP-ATP)*; NASA CR-4208; NASA LaRC: Hampton, VA, USA, 1989.
7. Yin, J.; Delfs, J. Improvement of DLR rotor aeroacoustic code (APSIM) and its validation with analytic solution. In Proceedings of the 29th European Rotorcraft Forum, Friedrichshafen, Germany, 16–18 September 2003.
8. NUMECA International. *FINE™/Acoustics Theoretical Manual (Release 8.1)*; NUMECA International: Brussels, Belgium, 2018.
9. ANSYS, Inc. *ANSYS Fluent Theory Guide*; ANSYS, Inc.: Canonsburg, PA, USA, 2021.
10. Free Field Technologies SA. *Actran 2020 User's Guide: Vol. 1—Installation, Operations, Theory and Utilities*; Free Field Technologies SA: Mont-Saint-Guibert, Belgium, 2019.
11. Farassat, F.; Brown, T.J. *A New Capability for Predicting Helicopter Rotor and Propeller Noise Including the Effect of Forward Motion*; NASA TM X-74037; NASA LaRC: Hampton, VA, USA, 1977.
12. NUMECA International. *FINE™/Turbo 14.2 User Guide*; NUMECA International: Brussels, Belgium, 2020.
13. Zhou, Y.C. Component-Level Model for Turbocharging Reciprocating Engine Propeller Propulsion System and Compressible Lifting Surface Inverse Method for Contra-Rotating Propfan. Ph.D. Thesis, Beijing University of Aeronautics and Astronautics, Beijing, China, 2016.
14. Sullivan, T.J. Aerodynamic performance of a scale-model, counterrotating unducted fan. *J. Turbomach.* **1990**, *112*, 579–586. [[CrossRef](#)]
15. Woan, C.J.; Gregorek, G.M. The exact numerical calculation of propeller noise. In Proceedings of the AIAA 11th Fluid and Plasma Dynamics Conference, Seattle, WA, USA, 10–12 July 1978.
16. Hirsch, C.; Ghorbaniasl, G.; Ramboer, J. Fan noise simulation in the time domain—Validation test cases. In Proceedings of the Fan Noise 2003 International Symposium, Senlis, France, 23–25 September 2003.
17. Wang, H.Y.; Shan, P.; Zhou, Y.C. Aerodynamic and discrete frequency noise characteristics of contra-rotating propfans under take-off conditions. *J. Aerosp. Power* **2023**, *submitted*. (In Chinese)

**Disclaimer/Publisher's Note:** The statements, opinions and data contained in all publications are solely those of the individual author(s) and contributor(s) and not of MDPI and/or the editor(s). MDPI and/or the editor(s) disclaim responsibility for any injury to people or property resulting from any ideas, methods, instructions or products referred to in the content.